Int J Thermophys (2015) 36:2486–2495
DOI 10.1007/s10765-015-1900-9

Investigations of Thermal, Optical, and Electric Properties as a Function of Composition for ZnS_xSe_{1-x} Crystals

D. Trefon-Radziejewska[1] · J. Bodzenta[1] · B. Toroń[1] · Ł. Drewniak[1] · A. Marasek[2]

Received: 13 February 2015 / Accepted: 5 May 2015 / Published online: 15 May 2015

Abstract ZnS_xSe_{1-x} single crystals with different S contents were examined. The crystals were grown by the modified Bridgman method. Thermal, optical, and electrical measurements for a solid solution of ZnS_xSe_{1-x} crystals are presented and analyzed to determine the influence of composition on the thermal diffusivity, the electrical resistivity, the relative permittivity, and the energy gap. The thermal measurement was based on the thermal wave method with detection using the mirage effect. For interpretation of the experimental data, a thermal model of a layered system was adopted. The results showed that the thermal diffusivity of samples decreases with an increase of the S content x. The electrical resistivity of investigated samples was measured by the constant voltage method. The relative permittivity was determined by dielectric spectroscopy and decreased with increasing sulfur content in the ZnSe. Further, the optical bandgap of ZnS_xSe_{1-x} was determined from photoluminescence spectra. Possible correlations between the thermal diffusivity, the optical bandgap, and electrical properties were studied. The obtained results showed a clear dependence of those parameters on the S concentration in the sample.

Keywords Photothermal wave method · II–VI Semiconductors · Thermal diffusivity · ZnSe

✉ D. Trefon-Radziejewska
Dominika.Trefon@polsl.pl

[1] Institute of Physics Center for Science and Education, Silesian University of Technology, Konarskiego 22B, 44-100 Gliwice, Poland

[2] Institute of Physics, Faculty of Physics, Astronomy and Informatics, Nicolaus Copernicus University, Grudziadzka 5, 87-100 Toruń, Poland

1 Introduction

Recently, much attention has been paid to II–VI mixed crystals for their potential applications in optoelectronic, photonic, and spintronic devices [1,2]. A promising candidate belonging to this group is zinc selenide—a semiconductor with a wide direct bandgap. ZnSe is suitable for short-wavelength optoelectronic device applications, especially in blue–green laser diodes, photodetectors, and tunable mid-IR laser sources for remote sensing [3,4]. The next II–VI crystal with an even wider gap energy than ZnSe is zinc sulfide. ZnS has attracted great interest for its applications in ultraviolet light-emitting diodes, flat panel displays, infrared windows, injections lasers, and many others [5,6].

What is more interesting, there is a possibility to create a ZnS_xSe_{1-x} solid solution by introducing sulfur ions into a ZnSe crystal lattice. The change in composition of the crystal influences its electronic properties, lattice parameters, and values of the energy gap. Especially, the application of bandgap engineering to ZnS_xSe_{1-x} ternary alloys gives the desired optical properties and results in developing optoelectronic and photonic devices with high performance [7–9].

However, it should be noted that also thermal properties change as a result of modification in the crystal composition. The introduction of even a small amount of foreign ions into the crystal structure deteriorates the heat transport due to the formation of defects in the crystal lattice. The significance of thermal phenomena becomes crucial in view of the miniaturization of semiconducting devices and the problem of heat dissipation. An important parameter of the material used in laser systems and other electronic devices is thermal diffusivity. It characterizes the speed of reaching a thermal equilibrium between a sample and its surroundings. In order to assure efficient heat transfer and also better control over crystal growth, the thermal diffusivity should be known.

Additionally, fabrication of green/blue lasers needs characterization of crystals for electrical and optical properties. Therefore, the aim of this work is determination of the thermal diffusivity of ZnS_xSe_{1-x} crystals with different S contents x and possible correlation with their electrical and optical parameters.

2 Measurements

2.1 Samples

Four samples of ZnS_xSe_{x-1} crystals were examined (for S content $x = 0, 0.1, 0.2$, and 0.3). Investigated crystals were grown from the melt by the high pressure (150 bar of argon)-modified Bridgman method using high-purity (99.995 %) powders of ZnSe and ZnS put in a graphite crucible in a stoichometric proportion [10]. The obtained crystal rods were about one centimeter in diameter and up to a few centimeters in length. The crystals were cut into about 0.1 cm thick disks of 0.8 cm diameter. Detailed information about the samples is collected in Table 1. The samples were not oriented to any crystallographic direction. The plates were mechanically ground and polished with diamond paste. For photoluminescence measurements, samples after polishing

Table 1 Basic information about samples with determined thermal diffusivities, energy gaps, electrical resistivities, and relative permittivities of investigated samples

Sample ZnS_xSe_{1-x}	#1	#2	#3	#4	#5
S content x	0	0.1	0.2	0.3	1
Thickness (cm)	0.114	0.135	0.137	0.142	–
Thermal diffusivity ($cm^2 \cdot s^{-1}$)	0.162	0.088	0.080	0.028	–
Energy gap (eV) (300 K)	2.71	2.76	2.84	2.89	3.67 [9]
Electrical resistivity (10^9 Ω·m)	4.97	7.91	14.7	10.3	–
Relative permittivity	11.0	10.5	9.75	9.50	9.0 [19]

were additionally chemically etched in a solution of sulfuric acid (96 %), potassium dichromate, and water.

2.2 Measuring Methods

2.2.1 Determination of Thermal Diffusivity

Photothermal methods are noncontact and very suitable methods for thermal characterization of semiconductors [11–13]. Thus, the thermal diffusivity was determined by a photothermal method with mirage detection. The scheme of measuring geometry is shown in Fig. 1. The sample was illuminated by a modulated light from a laser diode (808 nm). Each sample was covered with aluminum foil about 20 μm thick to improve light absorption. A probe beam from a He–Ne laser (7672 Lasos) passed near the heated surface and was deflected on a temperature gradient in the air above the sample. The deflection of the probe beam was detected by a position detector (DL400-7PSBA), and then the signal was sent to a lock-in amplifier (7265 DPS) to determine its amplitude and phase at the particular modulation frequency. More details about the experimental setup and mirage detection can be found elsewhere [14–16].

The thermal diffusivity was determined by using a 1D model of thermal wave propagation in the nth layered structure and a simplified description of light deflection

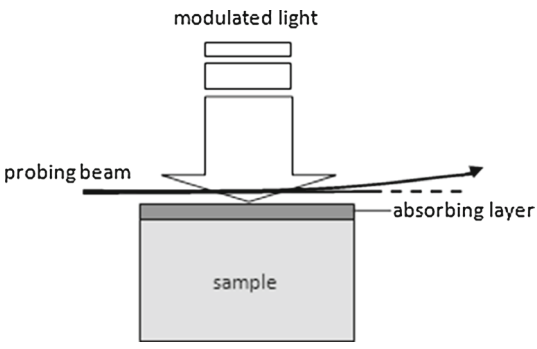

Fig. 1 Geometry of photothermal measurements with mirage detection

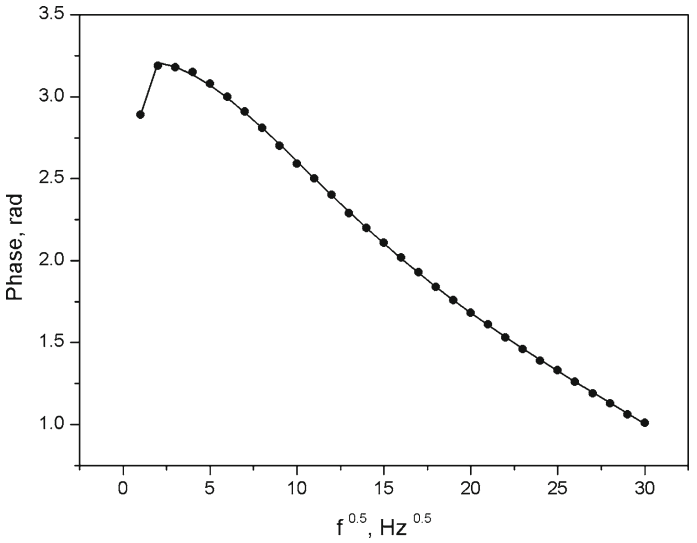

Fig. 2 Measured and fitted phase dependence on square root of modulation frequency of $ZnS_{0.2}Se_{0.8}$ sample

on the temperature gradient. For the probe beam passing above the sample surface in air, the deflection signal can be written as

$$S = -K\sqrt{\frac{\mathrm{i}\omega}{\alpha_\mathrm{a}}}\theta_0 \exp\left(-\sqrt{\frac{\mathrm{i}\omega}{\alpha_\mathrm{a}}}h\right), \tag{1}$$

where θ_0 is the temperature disturbance on the sample surface, α_a is the thermal diffusivity of air, h is the distance between the probe beam and the sample surface, K is a constant of proportionality, and ω is the modulation frequency. The temperature disturbance θ_0 depends on the thickness and thermal properties of layers (the thermal diffusivity and the thermal effusivity), optical properties of layers (the light absorption coefficient), and the modulation frequency ω. A detailed description of the model can be found in [14].

To obtain thermal diffusivities of investigated crystals, the measured dependences of the phase on the square root of the modulation frequency were fitted with dependences calculated using the presented model. The fitting procedures were written in MATLAB using its standard functions. An example result obtained for the $ZnS_{0.2}Se_{0.8}$ sample fitted with the theoretical curve is shown in Fig. 2.

2.2.2 Determination of Energy Gap

The energy gaps of ZnS_xS_{1-x} crystals were determined using photoluminescence spectroscopy. The experimental setup consisted of a HeCd laser (325 nm), a helium cryostat with sample, a temperature controller (LakeShore 331), and the spectrometer (MiroHR Horiba Jobin Yvon). The spectrometer included a filter wheel, diffraction

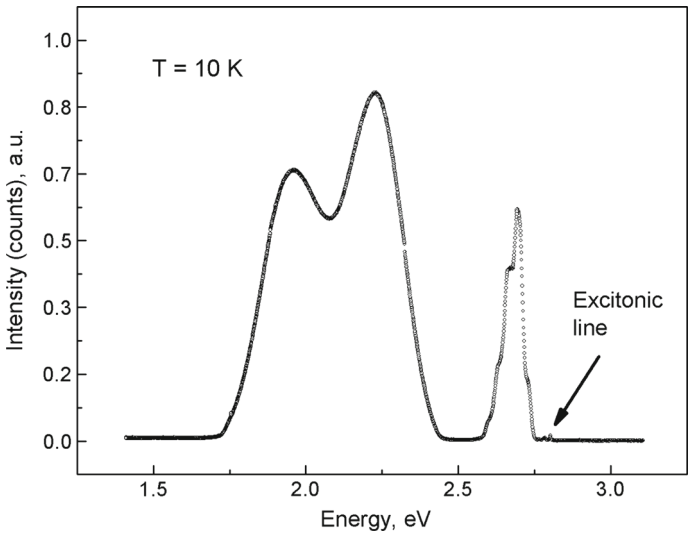

Fig. 3 Photoluminescence spectrum of ZnSe crystal at 10 K

gratings, and a thermoelectrically cooled CCD camera (Synapse Horiba Jobin Yvon) [10]. Measurements were provided in the temperature range from 10 K to 295 K and were controlled automatically. Figure 3 shows an example spectrum measured at 10 K, which is typical for II–VI mixed crystals. Such a spectrum consists of a high energy peak–exciton and edge emission with visible phonon structure below energy gap. The last component in the long wave region of a luminescence spectrum is connected with the existence of deep defects.

Excitonic energy gaps were determined from the maximum of the exciton emission dependence on temperature. Experimental data were interpreted using the following Varshni formula:

$$E_{\mathrm{g}}(T) = E_{\mathrm{g}}(0) - \frac{\gamma T^2}{\beta + T}, \tag{2}$$

where $E_{\mathrm{g}}(0)$ is the value of the bandgap at 0 K, whereas β and γ are constants connected with electron (exciton)–phonon interactions and the Debye temperature, respectively.

Figure 4 presents the temperature dependence of the exciton emission of the ZnSe crystal sample with fitting.

2.2.3 Determination of Electrical Resistivity and Relative Permittivity

The DC current–voltage characteristics were measured in order to determine the electrical resistivity of the investigated ZnS_xSe_{1-x} crystals. For this purpose, surfaces of the specimens were covered with silver contacts and connected to the Keithley 6517 A electrometer. The electrometer has been used as the bias source. Figure 5 shows typical

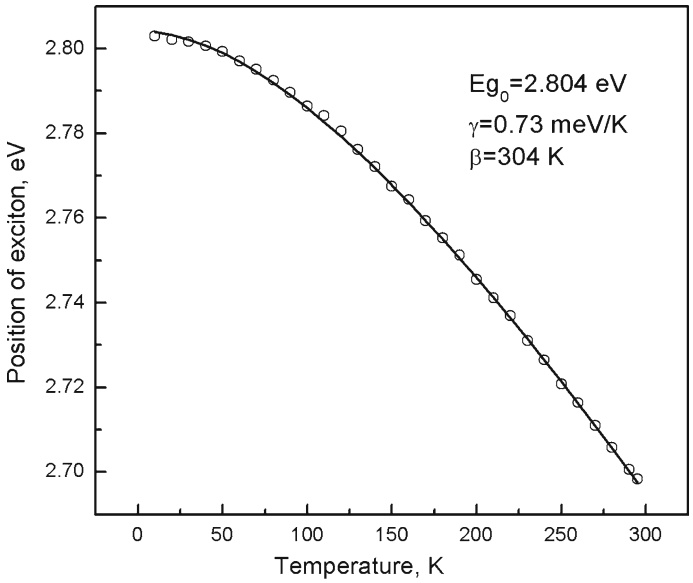

Fig. 4 Temperature dependence of the exciton emission of ZnSe crystal sample with fitting

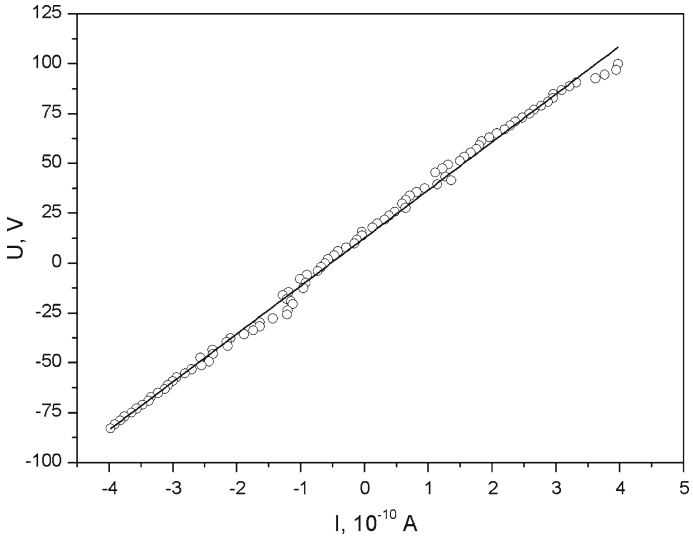

Fig. 5 DC current–voltage characteristic of $ZnS_{0.1}Se_{0.9}$ sample recorded at room temperature

DC current–voltage characteristic of the $ZnS_{0.1}Se_{0.9}$ sample recorded at room temperature. By a simple fit, one can get the resistance R of the crystal, and as a result, the electrical resistivity ρ from the formula,

$$\rho = R\frac{S}{d}, \tag{3}$$

where S is a surface of silver contact and d is the thickness of the sample.

Dielectric spectroscopy was used for determination of the relative permittivity ε_r of researched crystals. The relative permittivities were determined based on the measurements of a capacitance C by using the following equation:

$$C = \frac{\varepsilon_0 \varepsilon_r S}{d}, \tag{4}$$

The capacitance was measured as a function of frequency in the range from 100 Hz to 1 MHz by using the Agilent 4294A precision impedance analyzer. Changes in capacity were negligible, and therefore its value was read for a frequency of 1 kHz.

3 Results and Discussion

Results of thermal, optical, and electrical measurements obtained for all investigated samples are collected in Table 1. Thermal investigations indicate that the thermal diffusivity decreases with increasing content of sulfur in ZnS_xSe_{1-x} crystals. A similar behavior of the thermal diffusivity was observed previously for $Cd_xMn_{1-x}Te$ and $Cd_{1-x-y}Zn_xMg_ySe$ mixed crystals [17,18]. This dependency is shown in Fig. 6. It has to be emphasized that such an effect will not necessarily be true for the whole range of x (from 0 to 1). The introduction of a small amount of sulfur ions into a ZnSe crystal causes defects in the crystal lattice; thus, a decrease of the thermal diffusivity is observed. However, with the systematic and continuous replacement of Se with sulfur ions, the crystal structure starts to organize and eventually the thermal diffusivity can increase.

Estimated values of the energy gap as an increasing function of composition are presented in Fig. 7. Electrical measurements reveal that the electrical resistivity has

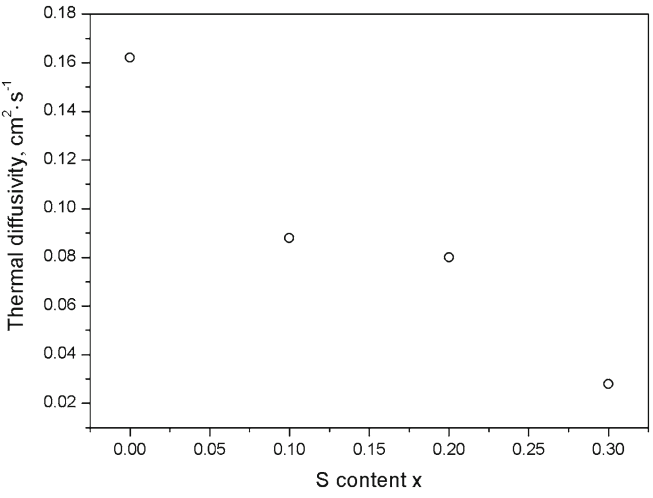

Fig. 6 Thermal diffusivity of ZnS_xSe_{1-x} crystals as a function of S content x

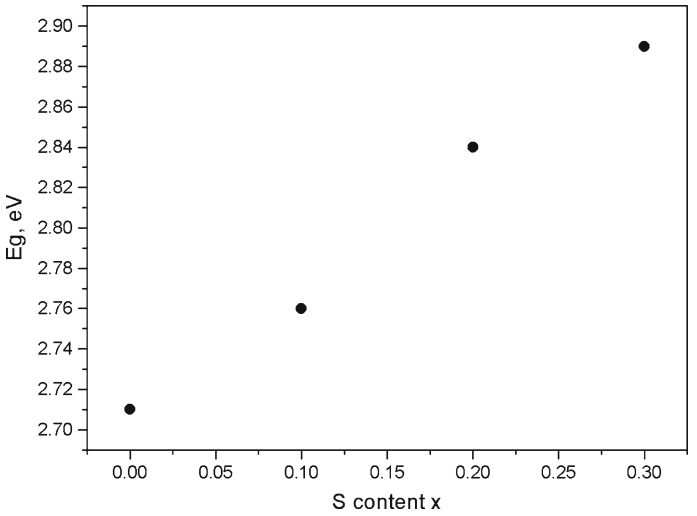

Fig. 7 Energy gap of ZnS_xSe_{1-x} crystals as a function of S content x

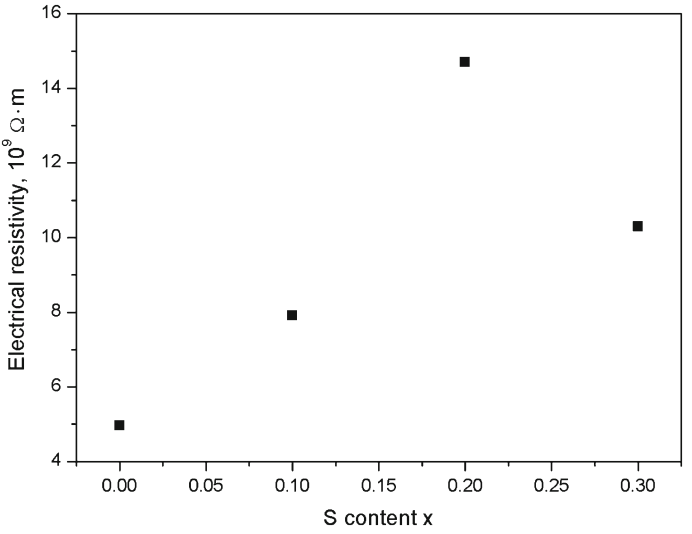

Fig. 8 Electrical resistivity of ZnS_xSe_{1-x} crystals as a function of S content x

an increasing tendency with growing x (Fig. 8). However, there is an unexpected result for the last sample—$ZnS_{0.3}Se_{0.7}$, because for an intrinsic semiconductor, the electrical resistivity should grow with an increase of the bandgap energy. Presumably, the reason of such behavior is that defects of the crystal structure in mixed crystals create additional energy levels in the bandgap. This leads to an increase in the charge carrier concentration.

Knowing the electrical resistivity, one can calculate the electrical conductivity of crystals. Subsequently, using the Wiedemann–Franz law, the relative contribution of

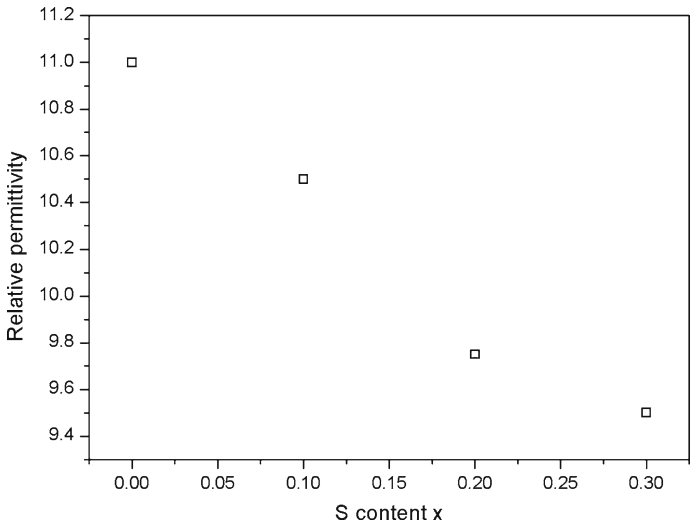

Fig. 9 Relative permittivity of ZnS_xSe_{1-x} crystals as a function of S content x

the charge carriers to the thermal conductivity can be estimated. It turns out that in the case of ZnS_xSe_{1-x} crystals, this contribution is negligible, and one can consider only the lattice thermal conductivity.

The relative permittivity of ZnS_xSe_{1-x} crystals is decreasing as a function of growing x and can be observed in Fig. 9.

4 Conclusion

A few samples of ZnS_xSe_{1-x} mixed crystals were examined to specify their thermal diffusivities, energy bandgaps, electrical resistivity, and relative permittivity. Obtained results show a clear dependence of investigated quantities on the S concentration in the sample. The thermal diffusivity and the relative permittivity decrease with growing S content x, whereas the energy bandgap and electrical resistivity increase.

Acknowledgment The authors from Silesian University of Technology acknowledge the financial support through statutory funds of the Institute of Physics Center for Science and Education.

References

1. A. Nurmikko, R. Gunshor, Semicond. Sci. Technol. **12**, 1337 (1997)
2. A. Waag, T. Litz, F. Fisher, H.J. Lugauer, T. Baron, K. Schull, U. Zehnoler, T. Gerchard, U. Lunz, M. Keim, R. Reuscher, G. Landwehr, J. Cryst. Growth **184–185**, 1 (1998)
3. A. Waag, F. Fisher, H.J. Lugauer, Th Litz, J. Laubender, U. Lunz, U. Zehnder, W. Ossau, T. Gerhardt, M. Moller, G. Landwer, J. Appl. Phys. **80**, 792 (1996)

4. Y. Zhu, Y. Bando, Chem. Phys. Lett. **377**, 367 (2003)
5. T.V. Prevenslik, J. Lumin. **87**, 1210 (2000)
6. T. Yamamoto, S. Kishimoto, S. Lida, Physica B **308**, 916 (2001)
7. M. Quillec, *Materials for Optoelectronics* (Kluwer Academic Publishers, Boston, 1996)
8. R.N. Dupuis, J.C. Campbell, J.R. Velebir, J. Cryst. Growth **77**, 598 (1986)
9. S. Adbi-Ben Nashrallah, S. Ben Afia, H. Belmabrouk, M. Said, Eur. Phys. J. B **43**, 3 (2005)
10. K. Strzałkowski, J. Zakrzewski, M. Maliński, Int. J. Thermophys. **34**, 691 (2013)
11. M. Pawlak, M. Maliński, Thermochim. Acta **599**, 23 (2015)
12. M. Pawlak, Appl. Phys. A **118**, 173 (2015)
13. K. Strzałkowski, M. Streza, M. Pawlak, Measurement **64**, 64 (2015)
14. J. Bodzenta, J. Mazur, A. Kaźmierczak-Bałata, Appl. Phys. B **105**, 623 (2011)
15. D. Korte-Kobylińska, R. Bukowski, B. Burak, J. Bodzenta, S. Kochowski, J. Appl. Phys. **100**, 063501 (2006)
16. A. Kaźmierczak-Bałata, J. Bodzenta, P. Szperlich, K. Wokulska, J. Kucytowski, T. Łukasiewicz, W. Hofman, J. Alloys Compd. **481**, 622 (2009)
17. K. Strzałkowski, F. Firszt, A. Marasek, Int. J. Thermophys. **35**, 2140 (2014)
18. K. Strzałkowski, Mater. Sci. Eng. B **184**, 80 (2014)
19. P. Kumar, A. Kumar, P.N. Dixit, T.P. Sharma, Indian J. Pure Appl. Phys. **44**, 690 (2006)